ISSN 0021-3640, JETP Letters, 2016, Vol. 103, No. 3, pp. 161–166. © Pleiades Publishing, Inc., 2016.

OPTICS AND LASER PHYSICS

Giant Red Shift of the Absorption Spectra Due to Nonstoichiometry in $GdCoO_{3-\delta}$[1]

S. G. Ovchinnikov[a, b], Yu. S. Orlov[a, b]*, A. A. Kuzubov[a], V. A. Dudnikov[a], A. E. Sokolov[a], V. N. Zabluda[a], S. B. Naumov[c], and N. P. Shestakov[a]

[a] *Kirensky Institute of Physics, Siberian Branch, Russian Academy of Sciences, Krasnoyarsk, 660036 Russia*
[b] *Siberian Federal University, Krasnoyarsk, 660041 Russia*
[c] *Siberian State Technological University, Krasnoyarsk, 660049 Russia*
** e-mail: jso.krasn@mail.ru*

Received November 23, 2015

The $GdCoO_{3-\delta}$ perovskite is a semiconductor with the energy gap $E_g \approx 0.5$ eV from electrical transport measurements. It reveals unusual optical absorption spectra without transparency window expected for semiconductors. Instead we have measured the narrow transmittance peak at the photon energy $\varepsilon_0 = 0.087$ eV. To reconcile the transport and optical data we have studied the effect of oxygen vacancies on the electronic structure of the $GdCoO_{3-\delta}$. We have found that oxygen vacancies result in the in-gap states inside the charge-transfer energy gap of the $GdCoO_3$. It is a multielectron effect due to strong electron correlations forming the electronic structure of the $GdCoO_{3-\delta}$. These in-gap states decrease the transparency window and result in a narrow absorption minimum. The predicted temperature dependence of the absorption spectra has been confirmed by our measurements.

DOI: 10.1134/S0021364016030115

Additionally to the interplay between spin, charge, and orbital degrees of freedom in all strongly correlated oxides, the rare-earth cobaltites $RCoO_3$ (R is 4*f*-element) reveal thermal fluctuations of the Co^{3+} spin value [1–3]. Thermal population of the excited magnetic states results in the spin-state transition. The signature for the onset of spin-state transition at $T_{onset} \sim 35$ K for $LaCoO_3$ can be found in magnetic susceptibility [4–7], heat capacity [5, 8], and thermal expansion [4]. The electron spin resonance [9], the X-ray absorption spectroscopy, and the X-ray magnetic circular dichroism [10] experiments have proved the high spin (HS) origin of the lowest excited state. Substitution of smaller R^{3+} for La in $RCoO_3$ results in the chemical pressure and stabilization of the low spin (LS) state due to an increase in the spin gap $\Delta_S = E_{HS} - E_{LS}$. This gap was estimated for all R ions from magnetic susceptibility data [11] and from the Birch–Murnaghan equation of state [12]. The $GdCoO_3$ compound has the spin gap value $\Delta_S(0) = 2300$ K [13]. With heating of the lattice, expansion results in a negative pressure that tends decreasing the spin gap. At $T_S = 800$ K the spin gap becomes zero. As concerns the charge gap, the measurements of the conductivity temperature dependence gives the activation energy at $T = 60$–100 K in the range $E_a = 0.2$–0.34 eV by different groups [14, 15]. Our calculation of the $GdCoO_3$ band structure by the multielectron LDA + GTB (local density approximation plus generalized tight binding) approach provides the charge-transfer gap $E_g \approx 0.5$ eV at $T = 0$ [13]. With such band gap one may expect the transparency window in the absorption spectrum with the absorption edge close to the E_g value.

In this paper we have measured the $GdCoO_3$ absorption spectra in the infrared region at temperatures $3.2 \text{ K} \leqslant T \leqslant 523$ K. Contrary to the expected transparency window we have found no window at all with a narrow transmittance peak at the photon energy $\varepsilon_0 = 0.087$ eV. To clarify the evident discrepancy between transport and optical data we have calculated density of states (DOS) of phonons and electrons. The ab initio calculations of phonon DOS were carried out within the framework of the density functional theory (DFT) in the generalized gradient approximation (GGA). Due to the strong electron correlations in $GdCoO_3$ conventional DFT approach fails. We calculated the electron DOS by the hybrid multielectron LDA + GTB approach that was developed to study the quasiparticle (QP) band structure in high-T_c cuprates [16, 17], manganites [18], and cobaltites [19]. While the LDA + GTB calculations revealed the insulator gap $E_g \approx 0.5$ eV for the stoichiometric $GdCoO_3$ [13],

[1] The article is published in the original.

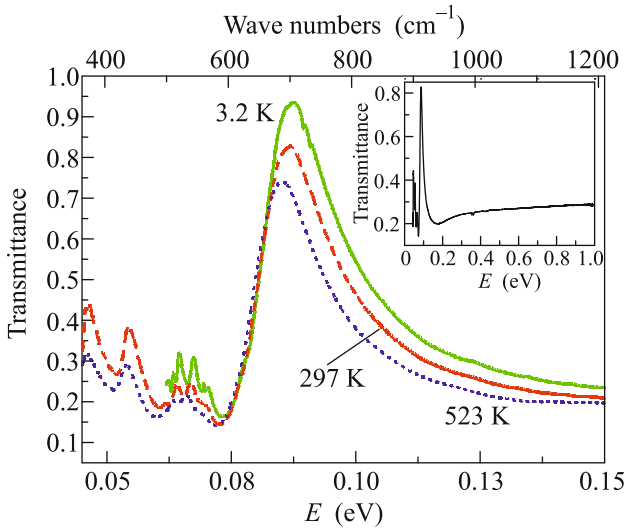

Fig. 1. (Color online) Transmittance spectrum of $GdCoO_{3-\delta}$, measured at T = (solid line) 3.2, (dashed line) 297, and (dark circles) 523 K. The room temperature transmittance in the wide energy region is shown in the inset to demonstrate the absence of any features at high energies.

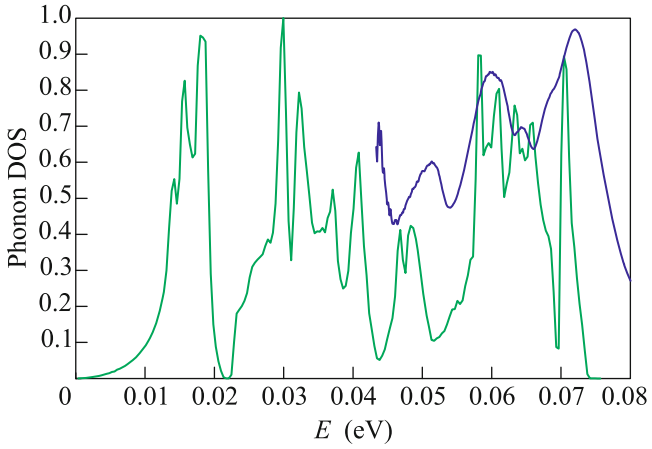

Fig. 2. (Color online) (Solid line) Phonon density of states from DFT calculations and (dashed line) the infrared part of absorption spectra measured at T = 523 K.

we found here the giant gap reduction due to the in-gap state formation below the bottom of the conductivity band. The origin of these in-gap states are oxygen vacancies due to nonstoichiometry. The formation of the in-gap states in the nonstoichiometric Mott insulators is a general phenomenon known for various strongly correlated oxides like cuprates, manganites, etc.

Polycrystalline samples of $GdCoO_{3-\delta}$ were prepared by the ceramic solid-state reaction technique. The oxygen content and nonstoichiometry index 6 were calculated using the value of mass loss measured by the thermogravimetric reduction [20]. The one was performed on a NETZSCH STA 449C analyzer equipped with an Aeolos QMS 403C mass spectrometer. According to the results of the thermogravimetric reduction the composition of gadolinium cobaltite is close to the stoichiometry of $GdCoO_3$, the 95% confidence interval for the oxygen index δ is 0.01. The full-profile crystal-structure analysis of $GdCoO_3$ was done in [13].

The infrared spectroscopy measurements were carried out with a vacuum Fourier transform infrared spectrometer Vertex 80v equipped with an RT-DLaTGS detector. Cryogenic measurements was carried out with cryostat type OptistatAC-V12 and Temperature Controller ITC503s by OXFORD Instruments in range 3.2–296 K. For temperature region 297–523 K, we used Variable temperature cell 147/QV High Stability Temperature Controller 4000 Series TM of Specac Ltd.

The transmittance spectrum of $GdCoO_{3-\delta}$, measured at T = 297 K is presented in the inset of Fig. 1. One can see, that transmittance spectrum consists of two parts, the low-energy (0.04–0.08 eV) and the high-energy (0.08–1.0 eV) parts and a narrow peak at the 0.085 eV. Since the high-energy part of the spectrum has no distinct features in Fig. 1 represents only the most informative part of this range at three temperatures. The low-energy part of the spectrum reveals the well-resolved vibrational excitations similar to those observed in the [21]. Figure 1 shows that heating from liquid helium temperature to 523 K shifts the narrow peak position by about 2 meV in the direction of decreasing energy.

To calculate phonon frequencies within the DFT approach, we used the plane-wave basis projector augmented wave method [22, 23] in the framework of the GGA in the Perdew–Burke–Ernzerhof form [24] as implemented in the VASP code [25–28]. Before calculation of the phonons, the structures were reoptimized. To calculate the phonon DOS, we have carried out the density-functional perturbation theory (DFPT) within supercell approach. Real-space force constants were calculated within the DFPT implemented in the VASP code [28], and phonon frequencies are calculated from the force constants using the PHONOPY package [29–31].

All calculated vibration frequencies lie in the range of 0.0724 eV (586 cm^{-1}) till 0.0142 eV (115 cm^{-1}) (Fig. 2). Group oscillations in the range of 0.0724 eV (586 cm^{-1})—0.0583 eV (469 cm^{-1}) represents the Co–O valence oscillations (stretching vibrations). The obtained splitting occurs due to the presence of the two types of cobalt–oxygen bonds. This is consistent with the results of experimental measurement of infrared spectra in the perovskite-type systems $RCoO_3$ [21], where it was shown the existence of such splitting

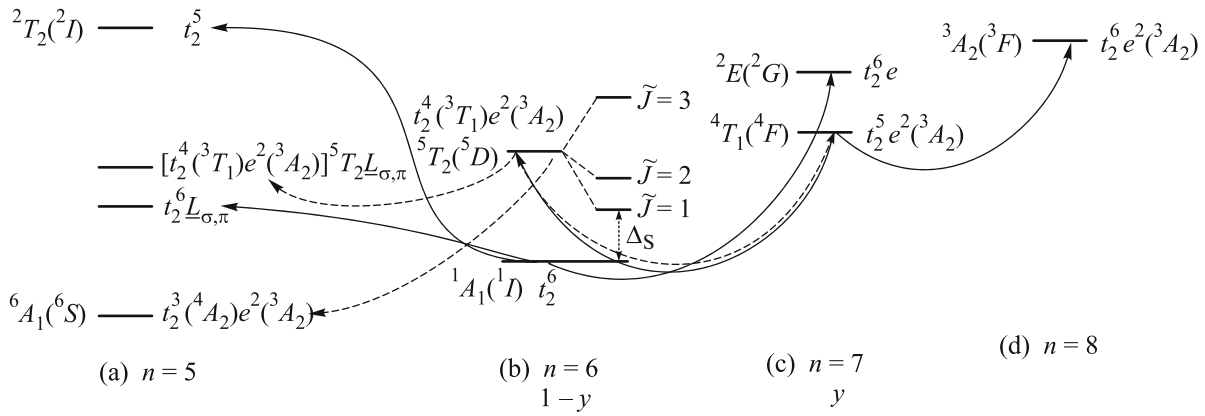

Fig. 3. Multielectron terms of CoO_6-cluster with (a) five, (b) six, (c) seven, and (d) eight electrons above the configuration $d^0(\mathrm{Co})p^6(\mathrm{O})$. For stoichiometric $GdCoO_3$ at $T=0$, only the lowest LS $d^6\,{}^1A_1$ term is occupied, all other terms unoccupied, but for nonstoichiometric crystal $Gd^{3+}Co^{3+}_{1-y}Co^{2+}_{y}Co^{2-}_{3-\delta}$ ($y=2\delta$) also HS $d^7\,{}^4T_1$ is occupied with filling factors $f^{\mathrm{LS}}_{\mathrm{Co}^{3+}}=1-y$ and $f^{\mathrm{HS}}_{\mathrm{Co}^{2+}}=y$, respectively. A set of Co^{3+} HS states split by the spin–orbit interaction is above the LS term with the spin gap $\Delta_S = E_{\mathrm{HS}} - E_{\mathrm{LS}}$. Electron addition $d^6 \to d^7$ and $d^7 \to d^8$ excitations forming the bottom of the conduction band and electron removal $d^6 \to d^5$, $d^7 \to d^6$ excitations forming the top of valence band are shown by solid lines. The dashed lines indicate the excitations responsible for the formation of band states upon the Co^{3+} HS thermal population.

of spectral lines, and its value increase with decreasing atomic radius of *f*-element. The vibrational modes in the interval 0.0497–0.0229 eV (401–184 cm^{-1}) are the mixture of the two types of oscillations: bending and translational motion of the cobalt atoms (external vibrations that correspond to the translational motion). Oscillations with a frequency less than 0.0211 eV (171 cm^{-1}) correspond to the translational motion of the atoms of gadolinium. From Fig. 2 we have concluded that the infrared absorption up to ≈0.08 eV results from phonon modes.

$GdCoO_3$ as well as other strongly correlated oxides is a difficult problem for the ab initio band theory. For example, LDA calculations incorrectly predict a metal for paramagnetic rare earth cobaltites $RCoO_3$ [32]. It is convenient to use the multiband *p–d* model as the starting model that reflects chemical structure of the cobaltites and strong electron correlations.

In the GTB approach, we consider electron as the linear combination of QPs, so-called Hubbard fermions, given by excitations between the different multielectron configurations obtained by exact diagonalization of the CoO_6-cluster. The QP spectral weight is determined by the occupation numbers of the initial and final local multielectron states for the given excitation. For more details of the method, see [33]. The low-energy eigenstates for nonstoichiometric $GdCoO_{3-\delta}$ compound are shown in Fig. 3. Here, $\underline{L}_{\sigma,\pi}$ is the spectroscopic notation of σ and π oxygen holes. To simplify the picture, the spin–orbit splitting is shown only for the high-spin state $^5T_{2g}$ (d^6 configuration). A set of Co^{3+} HS states is split by the spin–orbit interaction and lies above the LS term with the spin-gap $\Delta_S = E_{\mathrm{HS}} - E_{\mathrm{LS}}$. Here, the energy-level notations are the same as in the ionic model, but there are some eigenstates containing the oxygen hole admixture due to the covalence effect. The calculation of the eigenvectors for the CoO_6-cluster with the spin–orbit coupling and the Coulomb interaction has been done in [34].

We assume that eigenstates of neighboring cells are orthogonal. Otherwise (as in the case of cobaltites, where two neighboring CoO_6-clusters contain a common oxygen atom), an orthogonalization procedure should be done preliminary; that is, we have to construct a Wannier function in an explicit form instead of group oxygen orbitals. Such a procedure was first proposed for the three-band *p–d* model of cuprates [35] and then generalized to the multiband model [36]. With the Hubbard operators constructed using the exact cluster eigenstates, we can calculate the QP band structure for the infinite lattice in the multielectron LDA + GTB approach in the regime of strong electron correlations. The LDA + GTB method combines LDA band calculations with the GTB scheme [17], which is the implementation of Hubbard's ideas for multielectron and multiorbital systems. We use LDA functions to calculate the Wannier functions with the help of projection technique [37]. Single-electrons parameters of the tight binding Hamiltonian are calculated in the basis of these functions. It should be stressed that the LDA + GTB bands are not the single electron conventional bands. There is no any single particle Schrödinger equation with the effective potential. These QP are excitations between different

multielectron terms. The LDA + GTB bands depend on the multielectron term occupation numbers that should be calculated via the chemical potential equation. There is no rigid band behavior from the very beginning; the band structure depends on doping, temperature, pressure and external fields. Within the framework of the GTB approximation it has been shown [38, 39] that deviations of the electron concentration from an integral value results in localized levels of the impurity type emerging inside the semiconductor gap in spite of the lattice regularity. Following, we present the calculation results for nonstoichiometric $GdCoO_{3-\delta}$ with $\delta = 0.01$.

At temperature $T = 0$, only the ground term of the Co^{3+} ion (low-spin singlet $^1A_{1g}$) is populated in a stoichiometric $GdCoO_3$ crystal. The band structure is formed by the dispersion of the quasiparticle excitations d^6 $[^1A_1\ (t_2^6)] \to d^5$ $[^2T_2\ (t_2^5)]$, $[t_2^6 \underline{L}_{\sigma,\pi}]$ with the local energies $\Omega_{V_1} = E\ [d^6, {}^1A_1(t_2^6)] - E\ [d^5, {}^2T_2\ (t_2^5)]$, $\Omega_{V_2} = E\ [d^6, {}^1A_1\ (t_2^6)] - E\ [d^5, t_2^6 \underline{L}_{\sigma,\pi}]$, respectively, for the valence band and d^6 $[^1A_1\ (t_2^6)] \to d^7$ $[^2E\ (t_2^6 e^1)]$ for the conduction band with energies $\Omega_C = E[d^7, {}^2E(t_2^6 e^1)] - E\ [d^6, {}^1A_1\ (t_2^6)]$ (Fig. 3, solid lines). This multielectron approach was used in the X-ray spectroscopy (see, e.g., [40]). Due to the intercell hopping, the QP energy get the dispersion, $\Omega_m \to \Omega_m(k)$. The excitation energies determine the positions of the band centers. Obviously, the bands V and C are analogs of the lower and upper Hubbard subbands in the Hubbard model. The QP band structure corresponds to the charge-transfer insulator [41] with the gap $E_g \approx 0.5$ eV (Fig. 4a) at $T = 0$.

It is clear that the excitation from empty to empty terms has zero spectral weight. That is why nonzero spectral weight at $T = 0$ is related to the participation of the occupied LS Co^{3+} term; all possible excitations with nonzero weight are shown in Fig. 3 by solid lines. The excitations between LS d^6 and HS d^5 terms are forbidden by the spin conservation law (spin blockade according to Khomskii). In nonstoichiometric $Gd^{3+}Co^{3+}_{1-y}Co^{2+}_{y}Co^{2-}_{1-\delta}$ compound ($y = 2\delta$) at $T = 0$ both the ground terms (low-spin singlet $^1A_{1g}$) in Co^{3+} and (high-spin $^4T_{1g}$) in Co^{2+} ions are populated with filling factor $f_{Co^{3+}} = 1 - y$ and $f_{Co^{2+}} = y$, respectively. Partial occupation of the Co^{2+} HS states results in the substantial change of the QP spectrum. The d^7 $[^4T_1, t_2^5 e^2\ (^3A_2)] \to d^6$ $[^5T_2, t_2^4\ (^3T_1)\ e^2\ (^3A_2)]$ transitions are responsible for the appearance of the in-gap states (excitations that are higher in energy than V_1 and V_2, but lower than C) and for the insulator gap decrease (Figs. 4b and 4c).

When temperature increases, the thermal population of the Co^{3+} high-spin $^5T_{2g}$ term increases $\tilde{n}^{HS}_{Co^{3+}} = f_{Co^{3+}} n^{HS}_{Co^{3+}}$, resulting in contributions from possible excitations allowed by the selection rules for spin and spin projection ($\Delta S = \pm 1/2$, $\Delta S_z = \pm 1/2$), dashed lines in Fig. 3. Here, $n^{HS}_{Co^{3+}} = g_{HS}\exp(-\Delta_S/k_BT)/1 + g_{HS}\exp(-\Delta_S/k_BT)$, where g_{HS} is the degree of degeneracy of the $^5T_{2g}$ term. The spectral weight and the in-gap bandwidth are proportional to the sum $\tilde{n}^{HS}_{Co^{3+}} + \tilde{n}^{HS}_{Co^{2+}}$, $\tilde{n}^{HS}_{Co^{2+}} = f_{Co^{2+}} n^{HS}_{Co^{2+}}$. An increase in temperature leads to the fact that the bands formed by the transitions d^6 $[^5T_2, t_2^4\ (^3T_1)\ e^2\ (^3A_2)] \to d^7$ $[^4T_1, t_2^5 e^2\ (^3A_2)]$ begin increasing the width, and the insulator gap decreases. The quasiparticle spectrum and the insulator gap E_g are determined by the thermal population of the Co^{3+} HS state and, hence, by the spin gap Δ_S. Due to the temperature dependence Δ_S in $GdCoO_3$, the insulator gap E_g vanishes as temperature increases at $T_{IMT} \sim 780$ K [13]. For each temperature, the chemical potential and the QP band structure are calculated self-consistently. The QP band structures for $T = 300$ and 500 K are shown in Figs. 4d and 4e. The increase in spectral weight and in-gap bandwidth with increasing temperature is consistent with the experimentally observed shift of the transmission peak (Fig. 1) and a decrease in the transparency window. For better perception of it, in Fig. 4f we summarized and imposed the total DOSs in the vicinity of chemical potential for three different temperatures $T = 0$, 300, and 500 K (solid, dashed, and dotted line, respectively) and fixed $\delta = 0.1$ on an enlarged scale. As it seen, there is an increase in in-gap band with increasing temperature and a decrease in the transparency window at the same time.

According to Figs. 4c and 4e, the electron DOS has similar changes by increasing temperature at small nonstoichiometry or by increasing nonstoichiometry at small temperature.

Oxygen nonstoichiometry and the proximity of HS and LS states have a significant impact on the electronic structure of cobaltites and its temperature behavior. Dependence of the band structure on the temperature and the presence of in-gap states due to oxygen nonstoichiometry are essentially many-particle effects. While the stoichiometric $GdCoO_3$ has the charge transfer insulator gap 0.5 eV, the DOS in the nonstoichiometric compound has the in-gap contribution below the Fermi level, and this contribution increasing with the concentration of oxygen vacancies and temperature. The physical reason for the appearance of new levels and bands is the nonzero contribution from excited multielectron states to the single-particle DOS, which is absent in the stoichiometric case. In ordinary semiconductors, as is known, impu-

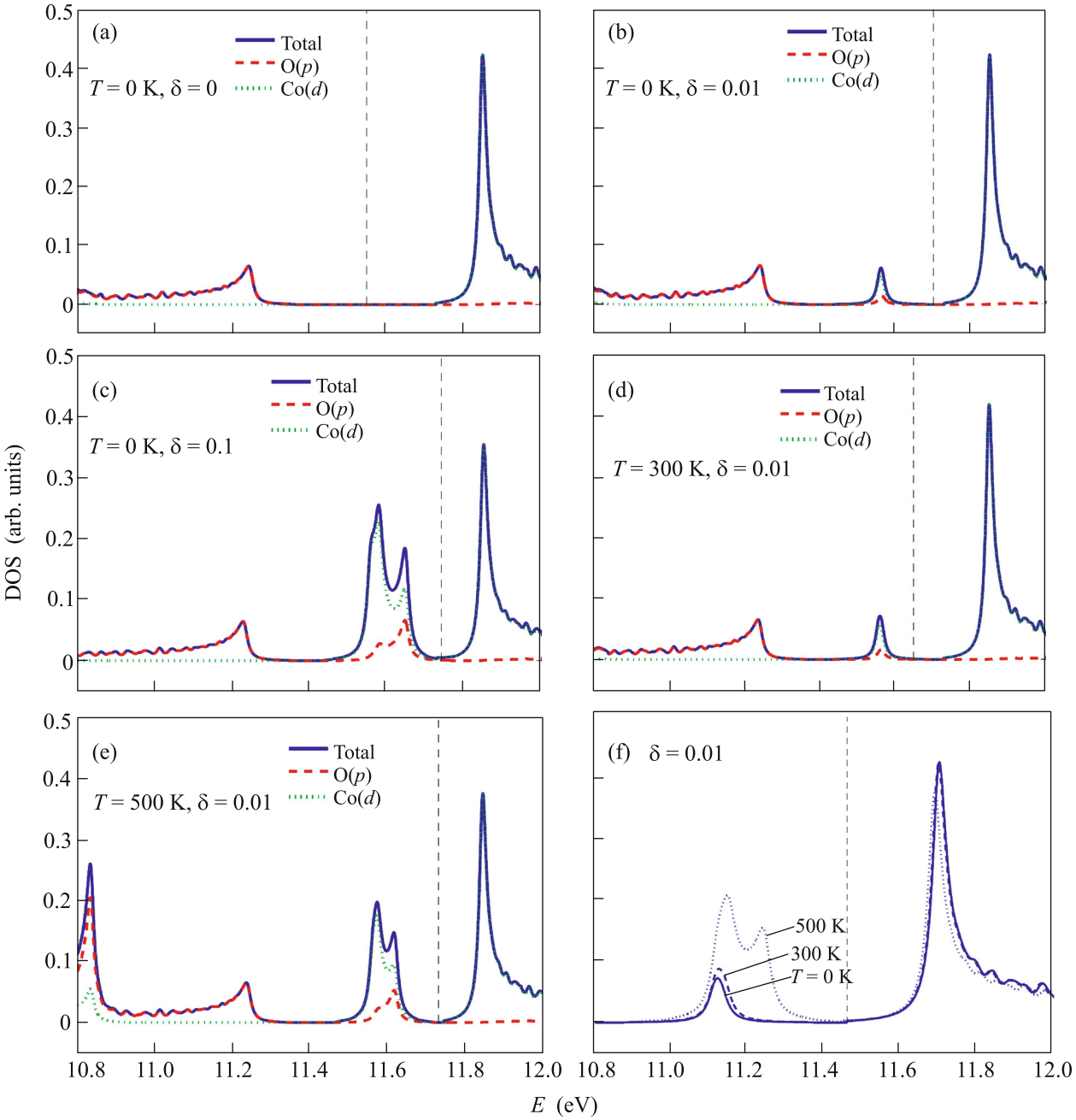

Fig. 4. (Color online) Total and partial densities of states (a) for the stoichiometric $GdCoO_3$ at $T = 0$ K and for the nonstoichiometric $GdCoO_{3-\delta}$ compound at $T =$ (b, c) 0, (d) 300, and (e) 500 K, calculated within the LDA + GTB. At $T = 0$, $GdCoO_3$ is an insulator with the gap $E_g \approx 0.5$ eV. At $\delta \neq 0$, the in-gap band appears below the conductivity band with the temperature dependent spectral weight and bandwidth. The dashed line shows the chemical potential. In panel (f), we summarize and impose the total DOSs in the vicinity of chemical potential for three different temperatures $T =$ (solid line) 0, (dashed line) 300, and (dotted line) 500 K and fixed $\delta = 0.1$ on an enlarged scale.

rity levels appear because of fluctuations of the crystal potential near a defect. As we saw the "impurity"-like levels can appear in the correlation semiconductors considered here even in the absence of such fluctuations. We assume that the only quantity varying due to the nonstoichiometry is the electron density, that all the parameters of the Hamiltonian are fixed, and that vacancies introduce no new terms into the Hamiltonian. Of course, in real material nonstoichiometry naturally introduces also fluctuations into the crystal potential, with the result in the QP scattering on these fluctuations. Hence, in calculating specific systems

this new mechanism should be taken into account along with the usual mechanism of scattering. The appearance of the in-gap states even for small vacancy concentration decreases the absorption edge up to the value of the order 10 meV, as can be seen from Figs. 4b and 4d. From the same Fig. 4 it is also clear that both the bottom of the conductivity band and the in-gap band are dominated by the *d*-electrons. The conductivity in the charge transfer insulator results mainly from the oxygen *p*-electrons, which is why the appearance of the in-gap states has no strong effect on the electrical conductivity. Thus, we can reconcile the emerging controversy of the transport and optical properties in the experimental studies of the $GdCoO_3$ samples with inevitable oxygen vacancies.

This work was supported by the Council of the President of the Russian Federation for Support of Young Scientists and Leading Scientific Schools (project no. NSh-2886.2014.2), by the Presidium of Russian Academy of Sciences (Program 34), by the Russian Foundation for Basic Research (project nos. 16-02-00507, 16-02-00273, 16-02-00098, and 14-02-00186), and by Internationale Büro, Bundesministerium für Bildung und Forschung (BMBF, grant no. 05K12GU2).

REFERENCES

1. S. Maekawa, T. Tohyama, S. E. Barnes, S. Ishihara, W. Koshibae, and G. Khaliullin, *Physics of Transition Metal Oxides* (Springer, Berlin, 2004).
2. N. B. Ivanova, S. G. Ovchinnikov, M. M. Korshunov, I. M. Eremin, and N. V. Kazak, Phys. Usp. **52**, 789 (2009).
3. S. R. Giblin, I. Terry, S. J. Clark, T. Prokscha, D. Prabhakaran, A. T. Boothroyd, J. Wu, and C. Leighton, Europhys. Lett. **70**, 677 (2005).
4. C. Zobel, M. Kriener, D. Bruns, J. Baier, M. Grüninger, T. Lorenz, P. Reutler, and A. Revcolevschi, Phys. Rev. B **66**, 020402 (2002).
5. T. Kyomen, Y. Asaka, and M. Itoh, Phys. Rev. B **67**, 144424 (2003).
6. J.-Q. Yan, J.-S. Zhou, and J. B. Goodenough, Phys. Rev. B **69**, 134409 (2004).
7. M. Magnuson, S. M. Butorin, C. Sathe, and J. Nordgren, Europhys. Lett. **68**, 289 (2004).
8. S. Stolen, F. Gronvold, H. Brinks, T. Atake, and H. Mori, Phys. Rev. B **55**, 14103 (1997).
9. S. Noguchi, S. Kawamata, K. Okuda, H. Nojiri, and M. Motokawa, Phys. Rev. B **66**, 094404 (2002).
10. M. W. Haverkort, Z. Hu, J. C. Cezar, T. Burnus, H. Hartmann, M. Reuther, C. Zobel, T. Lorenz, A. Tanaka, N. B. Brookes, H. H. Hsieh, H.-J. Lin, C. T. Chen, and L. H. Tjeng, Phys. Rev. Lett. **97**, 176405 (2006).
11. K. Knizek, Z. Jirak, J. Hejtmanek, M. Veverka, M. Marysko, G. Maris, and T. T. M. Palstra, Eur. Phys. J. B **47**, 213 (2005).
12. S. G. Ovchinnikov, Yu. S. Orlov, and V. A. Dudnikov, J. Magn. Magn. Mater. **324**, 3584 (2012).
13. Yu. S. Orlov et al., Phys. Rev. B **88**, 235105 (2013).
14. S. Yamaguchi, Y. Okimoto, and Y. Tokura, Phys. Rev. B **54**, R11022 (1996).
15. B. Scherrer, A. S. Harvey, S. Tanasescu, F. Teodorescu, A. Botea, K. Conder, A. N. Grundy, J. Martynczuk, and L. J. Gauckler, Phys. Rev. B **84**, 085113 (2011).
16. M. M. Korshunov, V. A. Gavrichkov, S. G. Ovchinnikov, Z. V. Pchelkina, I. A. Nekrasov, M. A. Korotin, and V. I. Anisimov, J. Exp. Theor. Phys. **99**, 559 (2004).
17. M. M. Korshunov, V. A. Gavrichkov, S. G. Ovchinnikov, I. A. Nekrasov, Z. V. Pchelkina, and V. I. Anisimov, Phys. Rev. B **72**, 165104 (2005).
18. V. A. Gavrichkov, S. G. Ovchinnikov, I. A. Nekrasov, and Z. V. Pchelkina, J. Exp. Theor. Phys. **112**, 860 (2011).
19. S. G. Ovchinnikov, Yu. S. Orlov, I. A. Nekrasov, and Z. V. Pchelkina, J. Exp. Theor. Phys. **112**, 140 (2011).
20. K. Conder, E. Pomjakushina, A. Soldatov, and E. Mitberg, Mater. Res. Bull. **40**, 257 (2005).
21. Y. Kim, D. H. Lee, T. Y. Kwon, and S. H. Park, J. Solid State Chem. **112**, 376 (1994).
22. P. E. Blochl, Phys. Rev. B **50**, 17953 (1994).
23. G. Kresse and D. Joubert, Phys. Rev. B **59**, 1758 (1999).
24. J. P. Perdew, K. Burke, and M. Ernzerhof, Phys. Rev. Lett. **77**, 3865 (1996).
25. G. Kresse and J. Hafner, Phys. Rev. B **48**, 13115 (1993).
26. G. Kresse and J. Furthmüller, Comp. Mat. Sci. **6**, 15 (1996).
27. G. Kresse and J. Furthmüller, Phys. Rev. B **54**, 11169 (1996).
28. G. Kresse, M. Marsman, and J. Furthmüller, VASP—Vienna Ab initio Simulation Package. http://cms.mpi.univie.ac.at/vasp.
29. A. Togo, L. Chaput, I Tanaka, and G. Hug, Phys. Rev. B **81**, 174301 (2010).
30. A. Togo, F. Oba, and I. Tanaka, Phys. Rev. B **78**, 134106 (2008).
31. A. Togo, http://phonopy.sourceforge.net.
32. P. Ravindran, P. A. Korzhavyi, H. Fjellvag, and A. Kjekshus, Phys. Rev. B **60**, 16423 (1999).
33. S. G. Ovchinnikov, V. A. Gavrichkov, M. M. Korshunov, and E. I. Shneyder, Springer Ser. Solid-State Sci. **171**, 143 (2012).
34. Yu. S. Orlov and S. G. Ovchinnikov, J. Exp. Theor. Phys. **109**, 322 (2009).
35. F. C. Zhang and T. M. Rice, Phys. Rev. B **37**, 3759 (1988).
36. L. F. Feiner, J. H. Jefferson, and R. Raimondi, Phys. Rev. B **53**, 8751 (1996).
37. V. I. Anisimov, D. E. Kondakov, A. V. Kozhevnikov, I. A. Nekrasov, Z. V. Pchelkina, J. W. Allen, S.-K. Mo, H.-D. Kim, P. Metcalf, S. Suga, A. Sekiyama, G. Keller, I. Leonov, X. Ren, and D. Vollhardt, Phys. Rev. B **71**, 125119 (2005).
38. S. G. Ovchinnikov, Sov. Phys. JETP **75**, 283 (1992).
39. S. G. Ovchinnikov, Phys. Usp. **40**, 993 (1997).
40. J. Zaanen and G. A. Sawatzky, J. Solid State Chem. **88**, 8 (1990).
41. J. Zaanen, G. A. Sawatzky, and J. W. Allen, Phys. Rev. Lett. **55**, 418 (1985).